Biomedical Optics EXPRESS

# *In vivo* layer-resolved characterization of oral dysplasia via nonlinear optical micro-spectroscopy

**Kert Edward,[1,*] Suimin Qiu,[2,5] Vicente Resto,[3,5] Susan McCammon,[3,5] and Gracie Vargas[1,4,5]**

[1]*Center for Biomedical Engineering, The University of Texas Medical Branch, Galveston, TX 77555, USA*
[2]*Department of Pathology, The University of Texas Medical Branch, Galveston, TX 77555, USA*
[3]*Department of Otolaryngology, The University of Texas Medical Branch, Galveston, TX 77555, USA*
[4]*Department of Neuroscience and Cell Biology, The University of Texas Medical Branch, Galveston, TX 77555, USA*
[5]*Center for Cancers of the Head and Neck, The University of Texas Medical Branch, Galveston, TX 77555, USA*
**k3edward@utmb.edu*

**Abstract:** Optical spectroscopy has proven to be a powerful technique for studying neoplastic transformation in epithelial tissue. Since specific intra-layer precancerous changes originate in the stratified layers of the oral mucosa, layer-resolved analysis will likely improve both our understanding of the mechanism of premalignant transformation, and clinical diagnostic outcomes. However, the native fluorescence signal in linear spectroscopy typically originates from a multi-layered focal volume. In this study, nonlinear spectroscopy was exploited for *in vivo* layer-resolved discrimination between normal and dysplastic tissue for the first time. Our results revealed numerous intra-layer specific differences.



**OCIS codes:** (170.5810) Scanning microscopy; (170.2520) Fluorescence microscopy; (170.6510) Spectroscopy, tissue diagnostics; (170.3880) Medical and biological imaging; (190.4180) Multiphoton processes.

## References and links

1. American Cancer Society, *Cancer Facts & Fig. 2011* (2011).
2. B. W. Stewart and P. Kleihues, eds., *World Cancer Report 2003* (International Agency for Research on Cancer, 2003).
3. B. W. Neville and T. A. Day, "Oral cancer and precancerous lesions," CA Cancer J. Clin. **52**(4), 195–215 (2002).
4. O. Kujan, R. J. Oliver, A. Khattab, S. A. Roberts, N. Thakker, and P. Sloan, "Evaluation of a new binary system of grading oral epithelial dysplasia for prediction of malignant transformation," Oral Oncol. **42**(10), 987–993 (2006).
5. H. Lumerman, P. Freedman, and S. Kerpel, "Oral epithelial dysplasia and the development of invasive squamous cell carcinoma," Oral Surg. Oral Med. Oral Pathol. Oral Radiol. Endod. **79**(3), 321–329 (1995).
6. P. M. Speight, "Update on oral epithelial dysplasia and progression to cancer," Head Neck Pathol. **1**(1), 61–66 (2007).
7. P. Nankivell and H. Mehanna, "Oral dysplasia: biomarkers, treatment, and follow-up," Curr. Oncol. Rep. **13**(2), 145–152 (2011).
8. H. M. Mehanna, T. Rattay, J. Smith, and C. C. McConkey, "Treatment and follow-up of oral dysplasia—a systematic review and meta-analysis," Head Neck **31**(12), 1600–1609 (2009).
9. J. E. Bouquot, P. M. Speight, and P. M. Farthing, "Epithelial dysplasia of the oral mucosa-Diagnostic problems and prognostic features," Curr. Diagn. Pathol. **12**(1), 11–21 (2006).
10. M. C. Skala, J. M. Squirrell, K. M. Vrotsos, J. C. Eickhoff, A. Gendron-Fitzpatrick, K. W. Eliceiri, and N. Ramanujam, "Multiphoton microscopy of endogenous fluorescence differentiates normal, precancerous, and cancerous squamous epithelial tissues," Cancer Res. **65**(4), 1180–1186 (2005).
11. I. Pavlova, M. Williams, A. El-Naggar, R. Richards-Kortum, and A. Gillenwater, "Understanding the biological basis of autofluorescence imaging for oral cancer detection: high-resolution fluorescence microscopy in viable tissue," Clin. Cancer Res. **14**(8), 2396–2404 (2008).
12. D. Shin, N. Vigneswaran, A. Gillenwater, and R. Richards-Kortum, "Advances in fluorescence imaging techniques to detect oral cancer and its precursors," Future Oncol. **6**(7), 1143–1154 (2010).

#162351 - $15.00 USD Received 31 Jan 2012; revised 15 May 2012; accepted 15 May 2012; published 12 Jun 2012

13. G. Zuccaro, N. Gladkova, J. Vargo, F. Feldchtein, E. Zagaynova, D. Conwell, G. Falk, J. Goldblum, J. Dumot, J. Ponsky, G. Gelikonov, B. Davros, E. Donchenko, and J. Richter, "Optical coherence tomography of the esophagus and proximal stomach in health and disease," Am. J. Gastroenterol. **96**(9), 2633–2639 (2001).
14. J. A. Evans, J. M. Poneros, B. E. Bouma, J. Bressner, E. F. Halpern, M. Shishkov, G. Y. Lauwers, M. Mino-Kenudson, N. S. Nishioka, and G. J. Tearney, "Optical coherence tomography to identify intramucosal carcinoma and high-grade dysplasia in Barrett's esophagus," Clin. Gastroenterol. Hepatol. **4**(1), 38–43 (2006).
15. C. Y. Wang, H. K. Chiang, C. T. Chen, C. P. Chiang, Y. S. Kuo, and S. N. Chow, "Diagnosis of oral cancer by light-induced autofluorescence spectroscopy using double excitation wavelengths," Oral Oncol. **35**(2), 144–150 (1999).
16. A. Gillenwater, R. Jacob, R. Ganeshappa, B. Kemp, A. K. El-Naggar, J. L. Palmer, G. Clayman, M. F. Mitchell, and R. Richards-Kortum, "Noninvasive diagnosis of oral neoplasia based on fluorescence spectroscopy and native tissue autofluorescence," Arch. Otolaryngol. Head Neck Surg. **124**(11), 1251–1258 (1998).
17. L. B. Lovat, K. Johnson, G. D. Mackenzie, B. R. Clark, M. R. Novelli, S. Davies, M. O'Donovan, C. Selvasekar, S. M. Thorpe, D. Pickard, R. C. Fitzgerald, T. Fearn, I. J. Bigio, and S. G. Bown, "Elastic scattering spectroscopy accurately detects high grade dysplasia and cancer in Barrett's oesophagus," Gut **55**(8), 1078–1083 (2006).
18. L. Qiu, D. K. Pleskow, R. Chuttani, E. Vitkin, J. Leyden, N. Ozden, S. Itani, L. Guo, A. Sacks, J. D. Goldsmith, M. D. Modell, E. B. Hanlon, I. Itzkan, and L. T. Perelman, "Multispectral scanning during endoscopy guides biopsy of dysplasia in Barrett's esophagus," Nat. Med. **16**(5), 603–606, 1p, 606 (2010).
19. R. A. Schwarz, W. Gao, D. Daye, M. D. Williams, R. Richards-Kortum, and A. M. Gillenwater, "Autofluorescence and diffuse reflectance spectroscopy of oral epithelial tissue using a depth-sensitive fiber-optic probe," Appl. Opt. **47**(6), 825–834 (2008).
20. M. C. Skala, G. M. Palmer, C. Zhu, Q. Liu, K. M. Vrotsos, C. L. Marshek-Stone, A. Gendron-Fitzpatrick, and N. Ramanujam, "Investigation of fiber-optic probe designs for optical spectroscopic diagnosis of epithelial pre-cancers," Lasers Surg. Med. **34**(1), 25–38 (2004).
21. A. Amelink, H. J. Sterenborg, M. P. Bard, and S. A. Burgers, "In vivo measurement of the local optical properties of tissue by use of differential path-length spectroscopy," Opt. Lett. **29**(10), 1087–1089 (2004).
22. W. Denk, J. H. Strickler, and W. W. Webb, "Two-photon laser scanning fluorescence microscopy," Science **248**(4951), 73–76 (1990).
23. L. Coghlan, U. Utzinger, R. Drezek, D. Heintzelmann, A. Zuluaga, C. Brookner, R. Richards-Kortum, I. Gimenez-Conti, and M. Follen, "Optimal fluorescence excitation wavelengths for detection of squamous intra-epithelial neoplasia: results from an animal model," Opt. Express **7**(12), 436–446 (2000).
24. T. J. Pfefer, L. S. Matchette, A. M. Ross, and M. N. Ediger, "Selective detection of fluorophore layers in turbid media: the role of fiber-optic probe design," Opt. Lett. **28**(2), 120–122 (2003).
25. J. Sun, T. Shilagard, B. Bell, M. Motamedi, and G. Vargas, "In vivo multimodal nonlinear optical imaging of mucosal tissue," Opt. Express **12**(11), 2478–2486 (2004).
26. G. Vargas, T. Shilagard, H. Ki-Hong, and S. McCammon, "Multiphoton autofluorescence microscopy and second harmonic generation microscopy of oral epithelial neoplasms," *in Annual International Conference of the IEEE Engineering in Medicine and Biology Society, 2009. EMBC 2009* (IEEE, 2009), pp.6611–6613.
27. M. C. Skala, K. M. Riching, A. Gendron-Fitzpatrick, J. Eickhoff, K. W. Eliceiri, J. G. White, and N. Ramanujam, "In vivo multiphoton microscopy of NADH and FAD redox states, fluorescence lifetimes, and cellular morphology in precancerous epithelia," Proc. Natl. Acad. Sci. U.S.A. **104**(49), 19494–19499 (2007).
28. S. Zhuo, J. Chen, X. Jiang, S. Xie, R. Chen, N. Cao, Q. Zou, and S. Xiong, "The layered-resolved microstructure and spectroscopy of mouse oral mucosa using multiphoton microscopy," Phys. Med. Biol. **52**(16), 4967–4980 (2007).
29. J. A. Gardecki and M. Maroncelli, "Set of secondary emission standards for calibration of the spectral responsivity in emission spectroscopy," Appl. Spectrosc. **52**(9), 1179–1189 (1998).
30. A. Pena, M. Strupler, T. Boulesteix, and M. Schanne-Klein, "Spectroscopic analysis of keratin endogenous signal for skin multiphoton microscopy," Opt. Express **13**(16), 6268–6274 (2005).
31. I. B. Gimenez-Conti and T. J. Slaga, "The hamster cheek pouch carcinogenesis model," J. Cell. Biochem. Suppl. **53**(S17F), 83–90 (1993).
32. A. Zoumi, A. Yeh, and B. J. Tromberg, "Imaging cells and extracellular matrix in vivo by using second-harmonic generation and two-photon excited fluorescence," Proc. Natl. Acad. Sci. U.S.A. **99**(17), 11014–11019 (2002).
33. J. A. Palero, H. S. de Bruijn, A. van der Ploeg-van den Heuvel, H. J. C. M. Sterenborg, and H. C. Gerritsen, "In vivo nonlinear spectral imaging in mouse skin," Opt. Express **14**(10), 4395–4402 (2006).
34. S. Huang, A. A. Heikal, and W. W. Webb, "Two-photon fluorescence spectroscopy and microscopy of NAD(P)H and flavoprotein," Biophys. J. **82**(5), 2811–2825 (2002).
35. M. Skala and N. Ramanujam, "Multiphoton redox ratio imaging for metabolic monitoring in vivo," in *Advanced Protocols in Oxidative Stress II* (Humana Press 2010), Chap.11, *http://www.springerprotocols.com/Abstract/doi/10.1007/978-1-60761-411-1_11*.
36. J. A. Palero, H. S. de Bruijn, A. van der Ploeg van den Heuvel, H. J. C. M. Sterenborg, and H. C. Gerritsen, "Spectrally resolved multiphoton imaging of in vivo and excised mouse skin tissues," Biophys. J. **93**(3), 992–1007 (2007).

#162351 - $15.00 USD Received 31 Jan 2012; revised 15 May 2012; accepted 15 May 2012; published 12 Jun 2012

37. D. L. Heintzelman, U. Utzinger, H. Fuchs, A. Zuluaga, K. Gossage, A. M. Gillenwater, R. Jacob, B. Kemp, and R. R. Richards-Kortum, "Optimal excitation wavelengths for in vivo detection of oral neoplasia using fluorescence spectroscopy," Photochem. Photobiol. **72**(1), 103–113 (2000).
38. R. Richards-Kortum and E. Sevick-Muraca, "Quantitative optical spectroscopy for tissue diagnosis," Annu. Rev. Phys. Chem. **47**(1), 555–606 (1996).
39. A. Uppal and P. K. Gupta, "Measurement of NADH concentration in normal and malignant human tissues from breast and oral cavity," Biotechnol. Appl. Biochem. **37**(1), 45–50 (2003).
40. N. J. Durr, C. T. Weisspfennig, B. A. Holfeld, and A. Ben-Yakar, "Maximum imaging depth of two-photon autofluorescence microscopy in epithelial tissues," J. Biomed. Opt. **16**(2), 026008 (2011).
41. W. Zheng, D. Li, S. Li, Y. Zeng, Y. Yang, and J. Y. Qu, "Diagnostic value of nonlinear optical signals from collagen matrix in the detection of epithelial precancer," Opt. Lett. **36**(18), 3620–3622 (2011).
42. Z. Zheng-Fei, L. Han-Ping, G. Zhou-Yi, Z. Shuang-Mu, Y. Bi-Ying, and D. Xiao-Yuan, "Second-harmonic generation as a DNA malignancy indicator of prostate glandular epithelial cells," Chinese Phys. B **19**(4), 049501 (2010).
43. J. Chen, S. Zhuo, R. Chen, X. Jiang, S. Xie, and Q. Zou, "Depth-resolved spectral imaging of rabbit esophageal tissue based on two-photon excited fluorescence and second-harmonic generation," New J. Phys. **9**(7), 212 (2007).
44. D. C. G. De Veld, M. J. Witjes, H. J. Sterenborg, and J. L. Roodenburg, "The status of in vivo autofluorescence spectroscopy and imaging for oral oncology," Oral Oncol. **41**(2), 117–131 (2005).

## 1. Introduction

According to the most recent report by the American Cancer Society, an estimated 39,400 new cases of oral and pharyngeal carcinoma occurred in the US in 2011, which resulted in almost 8000 deaths [1]. Despite the relative ease of access to the oral cavity and the high success rate for the treatment of localized malignancies, oral cancer is still the 11th most prevalent form of cancer [2]. The 5-year survival rate for early stage malignancies is approximately 80% but can be as low as 19% for cases with metastasis [3]. Thus the early detection and treatment of oral squamous cell carcinoma (OSCC), which accounts for 96% of oral cancers, is critical to reduced morbidity and mortality. Oral malignancy progresses in a multistep process that begins with premalignant alterations of the oral mucosa. In particular, oral dysplasia is of significant interest as it is associated with a high malignant transformation rate, depending on the severity [4,5]. For example, severe dysplasia has a reported malignancy transformation rate up to 50%, moderate dysplasia varies from 3% to 15%, while mild dysplasia has a very low risk of less than 5% [6]. Although clinically observable conditions including leukoplakia and erythroplakia can be indicators of dysplasia, dysplasia itself cannot be detected visually. At present, histological grading subsequent to biopsy remains the primary determinant of potential pre-malignant or malignant change [2]. Given the likelihood of transformation for advanced dysplasia, a recommended treatment for premalignancy is the surgical excision of high risk lesions [7,8]. However, success is dependent upon accurate identification of these sites of interest.

The progression to pre-cancer and cancer involves a complex series of biochemical and morphometric changes occurring at multiple layers throughout the oral mucosa [5,9]. Some of the earliest known alterations originate near the basement membrane and progress towards the surface [9]. Early alterations in the extracellular matrix also occur in the stroma, some of which may even precede epithelial alterations [5]. However, clinical diagnosis of premalignancy and malignancy typically involves white light inspection of suspicious sites, which essentially precludes subsurface interrogation. Layer-resolved analysis could potentially improve noninvasive diagnosis of treatable precancerous lesions and early cancers as a consequence of the likely earlier detection compared to characterization based on surface alterations or bulk properties. An enhanced understanding of neoplastic progression is yet another potential benefit of layer-resolved evaluation of dysplastic mucosa.

The autofluorescence of native biochemicals and tissue constituents including collagen in precancerous and cancerous tissue including the oral mucosa has been shown to be sensitive to neoplastic change [10,11]. Several imaging [11–14] and spectroscopy techniques [15–18] based on this principle have been exploited as non-invasive diagnostic approaches for *in vivo* microscopic examination of suspicious sites. Significant promise has been shown in clinical

#162351 - $15.00 USD Received 31 Jan 2012; revised 15 May 2012; accepted 15 May 2012; published 12 Jun 2012

studies particularly with regard to optical spectroscopy [19,20] and it is conceivable that this technique may eventually obviate or more likely, significantly reduce the need for biopsies. However, single photon (1P) or linear spectroscopy is encumbered by two main limitations. Firstly, signal acquisition depth is restricted due to the high scattering associated with the UV excitation. Optical penetration in dysplastic tissue is further limited by attenuation due to thickening of the epithelium, increased scattering associated with intracellular morphologic changes and absorption due to increased micro-vascularity [21]. Secondly, (1P) excitation elicits fluorescence from an extended excitation volume [22]. This effect is substantially mitigated in confocal fluorescence microscopy but at the expense of signal intensity. Achieving an optimal balance between these competing parameters in 1P spectroscopy usually means that localized excitation is compromised, resulting in bulk excitation. In the case of the oral mucosa, statistical approaches for decoupling the stratum corneum, epithelium and stromal emission contribution, including principle component analysis [23], have been investigated. A priori information is however often required and the results are difficult to validate. In recent years, several approaches have been proposed for "depth-sensitive" fiber-based spectroscopy including the use of ball lens coupled fiber optic-probes [19], angled illumination [20], multiple point signal collection away from excitation probe [24], and differential path-length spectroscopy [21]. In each instance, only approximate depth sensing (i.e. shallow, medium, deep) was possible.

In this work the spectroscopic characteristics of oral dysplasia were investigated using *in vivo* layer and intra-layer resolved two-photon micro-spectroscopy. This approach exploits the inherent advantages of two-photon compared to 1P microscopy which includes superior penetration depth, reduced photo-damage due to near-infrared excitation and highly localized excitation volumes [22]. While two-photon microscopy has been investigated for evaluating normal oral mucosa [25], morphometric change with oral neoplasia [26], as well as image-based redox measurement [27], two-photon spectroscopy has been restricted to the study of normal oral mucosa [28]. This research presents an initial summary of some of the non-linear spectroscopic changes observed in each of the stratified layers of the oral mucosa in normal and dysplastic oral mucosa.

## 2. Method and materials

### *2.1. Multiphoton imaging/ spectroscopy system*

Multiphoton imaging and spectroscopy were performed using a custom-built system [25] with an incorporated spectrometer. The spectrometer consisted of a spectrograph (Acton Research Corporation, Spectra Pro 150) with a calibrated EM CCD camera (Newton, Andor, Ireland) used for detecting and recording spectral information. Figure 1 depicts a schematic of the experimental setup. A Ti:sapphire femtosecond (~100fs, 82MHz) laser (Tsunami, Spectra-Physics, CA) tunable from ~690 nm to 900 was used as the excitation source.

The spectral resolution of the spectroscopy system was 0.1nm per pixel in the spectral window 200 nm-700 nm. A 300g/mm grating was utilized and the entrance slit separation was maintained at 0.25 mm for all measurements. Prior to spectral data acquisition, calibration was performed using a Mercury-argon light source. The spectral transmission properties of the dichroic and optics (lenses, mirrors, filters etc.) of the microscopy system was determined and used to correct all measured emission spectra. An additional flat field correction was made for the wavelength dependence of the CCD camera using two standard fluorophores [29]. All recorded spectra were background corrected and subsequently processed for the removal of sharp spikes due to cosmic rays. An integration time of 10 seconds was used for spectra acquisition in all instances.

A translation mirror in the detection path selectively directed the emission signal from the sample to either a photo-detector for imaging or to the spectroscopy setup. The incident power on the sample was maintained at 24 mW during signal acquisition. A 40X, 1.2 NA water

#162351 - $15.00 USD Received 31 Jan 2012; revised 15 May 2012; accepted 15 May 2012; published 12 Jun 2012

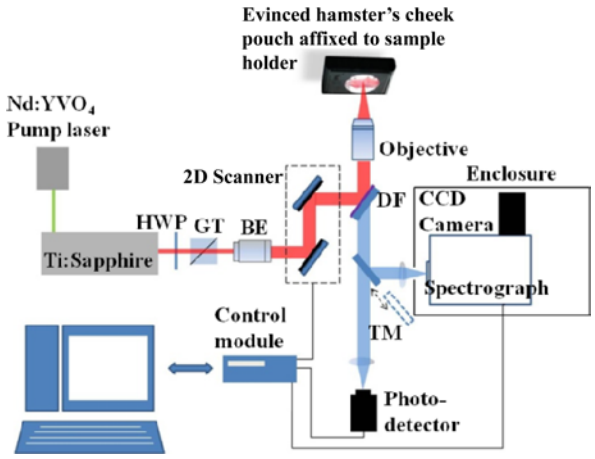


Fig. 1. Diagram depicting experimental setup for *in vivo* two photon autofluorescence spectroscopy and imaging. HWP: half wave plate; GT: Glans Thompson prism; BE: beam expander; DF: dichroic filter; TM: translational mirror.

immersion lens (C-Apochromat) objective was utilized for both imaging and spectroscopy. In imaging mode, broadband emission in the range 400-650 nm was collected. The acquired 2P images presented are morphologically representative of the different tissue classifications investigated and consistent with previously published results [10,25,26].

### *2.2. Animal model*

A Golden Syrian hamster model for oral precancer was utilized in this study [30]. This model follows the transformation of oral mucosa from normal to precancer to squamous cell carcinoma in a manner analogous to that in humans [31]. The right buccal pouch of the hamsters was treated by thrice-weekly topical application of 0.5% 9, 10-dimethyl-1, 2-benzanthracene (DMBA) for 6-7 weeks to induce dysplasia (n = 4). Controls were untreated (n = 4). Prior to spectral interrogation and imaging, each animal was anesthetized with a mixture of 150 mg/kg ketamine and 2.5 mg/kg xylazine via intraperitoneal injection. The buccal pouch was everted, rinsed with distilled water and attached to a sample holder for imaging. Spectroscopy results and multiphoton images were obtained from three sites for each animal (12 DMBA-treated sites and 12 sites from control animals). At each site, the stratum corneum, superficial and basal epithelium, and submucosal stroma were each investigated at 780 nm, 800 nm, 840 nm and 890 nm excitation. Pilot assessments of the variability between the three sites were conducted in which multiple measurements were acquired and tested for significant differences via ANOVA analysis. The difference (peak position and spectral distribution) between the normalized three spectra acquired at each site was not statistically significant, although a slightly greater variation was observed for dysplasia than for normal tissue. This was true even for sites containing morphometric variation as revealed from 2P imaging. Imaged sites were biopsied, fixed in 10% neutral-buffered formalin, embedded in paraffin and transversely sectioned. Each section was stained using hematoxylin-eosin (H&E) and graded by a pathologist (SQ) for histological stage (normal, moderate dysplasia, severe dysplasia). All studies were approved by the Institutional Animal Care and Use Committee at the University of Texas Medical branch and conformed to the Guide for the Care and Use of Laboratory Animals.

### *2.3. Data analysis*

All data processing to assess spectroscopic intensity and spectral differences was performed using proprietary code written in Matlab. Intensity data was obtained from the spectral plots

#162351 - $15.00 USD Received 31 Jan 2012; revised 15 May 2012; accepted 15 May 2012; published 12 Jun 2012

by integrating the area below the curve. Statistical comparison between normal and dysplastic groups (moderate, severe) was achieved by ANOVA followed by Tukey's post hoc test.

## 3. Results

### *3.1. Oral mucosa histopathology*

Representative images of H&E stained sections for each grading are shown in Figs. 2(a)–2(c) with the three main stratified layers of interest represented in image (a). The stratum corneum is composed primarily of dead cornified cells which have migrated to the surface and has a uniform thickness of about 10-15 μm in the oral mucosa of normal hamsters [25]. In Fig. 2(a), the basal layer is identified by the dotted green line. Immediately below this layer is the submucosal stroma which is includes type I collagen, elastin and fibroblasts. Normal mucosa is characterized by uniform, well-defined layers as shown in Fig. 2(a). Dysplastic tissue however, is characterized by changes in the stratified layers including thickening of the stratum corneum (hyperkeratosis), the appearance of prickle cells in this outer layer (parakeratosis) which is apparent from the presence of nuclei in this normally anuclear layer, the proliferation of cells from the basal layer throughout the thickness of the epithelium, and the disruption of the usual boundaries which separate the layers. The latter is evident in the basal layer of Fig. 2(c). In moderate dysplasia basal cell proliferation is present in approximately the lower two-thirds of the epithelium whereas the full epithelium is involved in severe dysplasia.

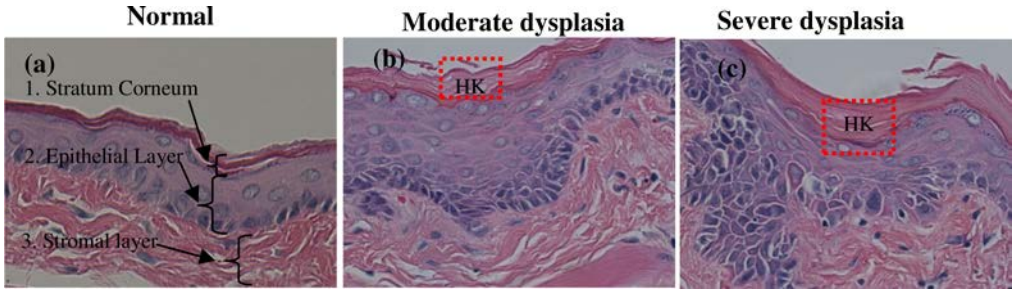


Fig. 2. Cross-sectional H&E sections of normal (a), moderate dysplasia (b) and severe dysplasia (c) for hamster oral mucosa. The region above the basal layer in figure (a) represents the epithelium with the stroma represented by the structure below this layer. The dysplastic specimens are characterized by significant changes including a thickening of the stratum corneum (hyperkeratosis) HK which is observed in figures (b) and (c).

### *3.2. Stratum corneum*

In Fig. 3, representative *in vivo* 2P micrographs at 780 nm excitation of the stratum corneum for normal (n = 12), moderate (n = 4) and severe dysplasia (n = 4) of the oral mucosa are depicted. Two of the 12 DMBA treated sites were graded as mild (not included) and two samples could not be assigned a definitive grade. Mild dysplasia is associated with a low rate of transformation to OSCC and is not of significant clinical interest. This grade was therefore not included in this study. Several reports on the observed differences in the stratum corneum with premalignant and malignant changes have been reported [10,26,32,33]. These include reduced autofluorescence intensity and irregularly shaped keratinocytes, which were observed quantitatively in the current study. Normalized averaged spectroscopy results for normal and two grades of dysplasia are presented in Fig. 3(d) for 780 nm excitation.

The spectrum for normal stratum corneum (black) is more symmetric with a peak at approximately 515 nm whereas the emission spectra is asymmetric and blue-shifted by approximately 30 nm relative to normal in the case of dysplasia. As shown in plot 3(e), the magnitude of the blue shift is observed to decrease with excitation wavelength up to 860 nm, after which a slight red shift was recorded. This difference was statistically significant at all

#162351 - $15.00 USD Received 31 Jan 2012; revised 15 May 2012; accepted 15 May 2012; published 12 Jun 2012

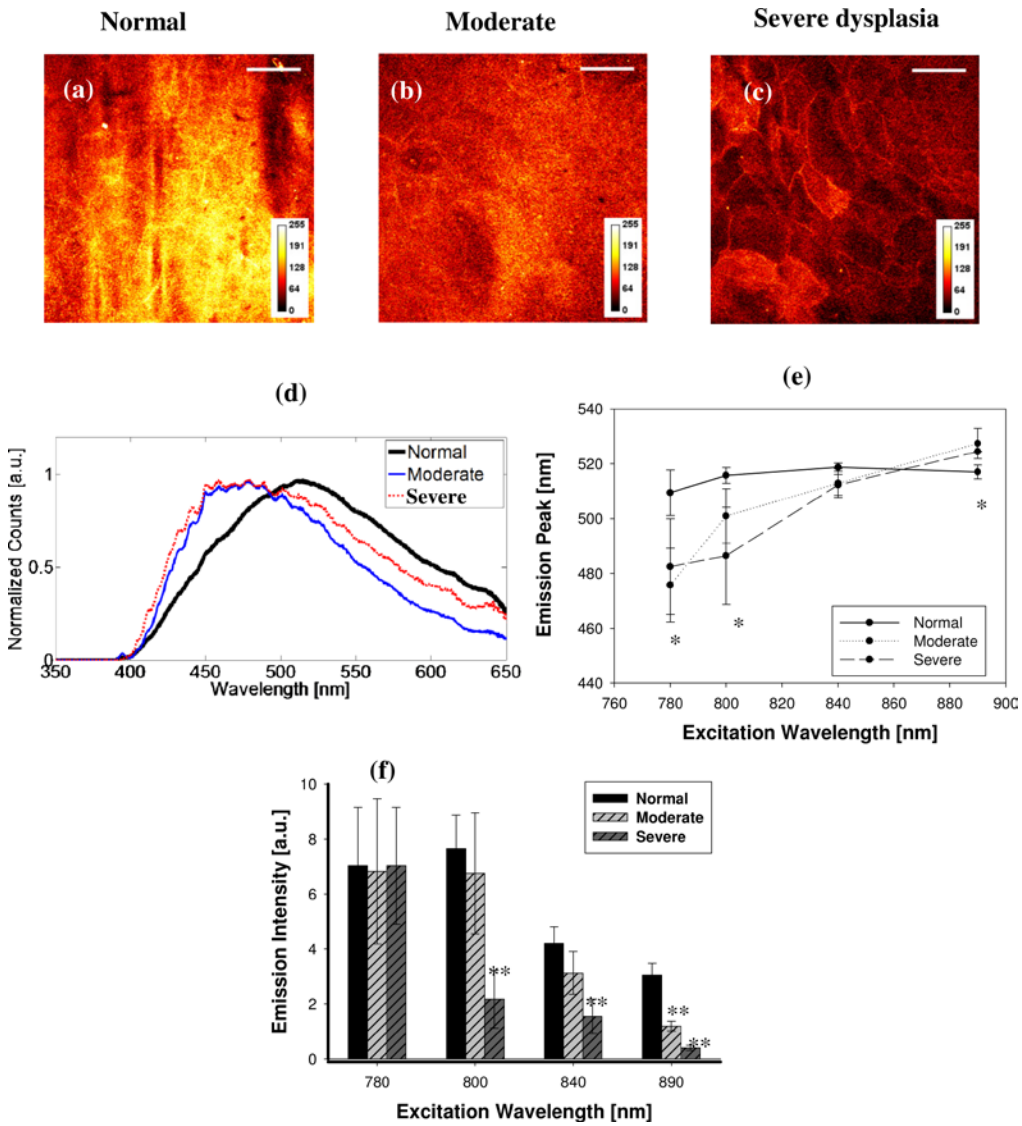


Fig. 3. 2P micrographs of the stratum corneum of the oral mucosa for (a) normal, (b) moderate and (c) severe dysplasia (Scale bar in a-c is 50 μm). Representative spectra from each of these three groups is shown in (d) for 780 nm excitation. Plot (e) represents the emission peak position with respect to excitation wavelength for the three groups with standard error bars. For each grading classification, the total emission intensity at 780 nm to 890 nm excitation is shown in (f). The error bar in (e) represents the standard error. Level of significance is shown for moderate and severe relative to normal *($p < 0.05$), ** ($p < 0.001$).

wavelengths except 840 nm. While differentiation between normal and dysplastic oral mucosa is possible based on the emission peak position, this parameter did not allow for discrimination between the dysplastic groups. The total emission intensity from the stratum corneum as a function of excitation wavelength is shown in Fig. 3(f) for the different classification of oral mucosa. An overall decrease in the emission intensity is observed with both the progression of dysplasia and the increase in the excitation wavelength. Statistically significant differences in intensity between the normal and dysplastic mucosa occurred at 800, 840, 890 nm excitation, with the most pronounced differences observed at the latter wavelength.

#162351 - $15.00 USD Received 31 Jan 2012; revised 15 May 2012; accepted 15 May 2012; published 12 Jun 2012

*3.3. Epithelium*

*In vivo* 2P autofluorescence representative images of the superficial (Figs. 4(a)–4(c)) and basal epithelium (Figs. 4(d), 4(e)) are shown in Fig. 4 for 780 nm excitation. The latter corresponds to the region of the mucosa directly at the epithelial-stromal interface while the former defines the region directly below the stratum corneum. This distinction is made in light of the fact that histological changes in pre-neoplasia begin at the basal layer and progress upward. It may therefore be possible to detect precancerous changes in the basal but not the superficial epithelium.

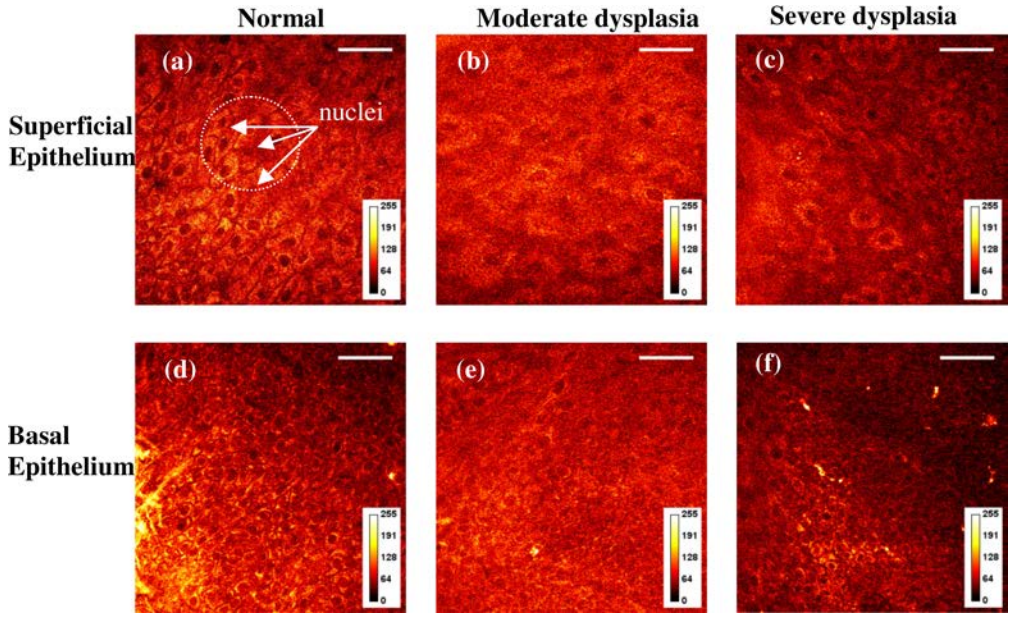


Fig. 4. Images (a)–(c) are *in vivo* 2P micrographs of normal, moderate dysplasia and severe dysplasia respectively, of the superficial epithelium of the oral mucosa at 780 nm excitation. The results for the basal layer are represented in images (d)–(f). The dotted white circle in (a) represents a collection of prickle cells in which the dark elliptical centers correspond to the nuclei. The cytoplasm of these cells is bright relative to the nuclei. Scale bar in a–f is 50 μm.

Dark elliptical circles present in each of the images indicate the position of the nuclei of prickle cells. An overall increase in nuclear size is observed with the progression from normal to severe dysplasia. In the basal epithelium, an increase in the cellular density is apparent with the progression to severe dysplasia. The spectroscopic features of superficial and basal epithelium are shown in Fig. 5. In the superficial epithelium, a blue shift of approximately 35 nm is observed between the emission spectra of the dysplastic mucosa relative to the normal at 780 nm excitation as shown in Fig. 5(a).

This is confirmed in Fig. 5(c) and Fig. 5(d) where it is also apparent that the blue shift in both layers decreases with excitation wavelength. In the epithelium, the shift in the emission spectrum between normal and dysplasia is significant at 780 nm and 840 nm ($p < 0.001$). It was also possible to differentiate between moderate and severe dysplasia at these two wavelengths ($p < 0.05$). The normalized emission curves for the dysplastic tissue are identical below approximately 460 nm for both investigated regions of the epithelium but a consistently higher intensity was detected for moderate dysplasia above this wavelength (5a and 5b). This observation will be further highlighted in the discussion section. A statistically significant decrease in the emission intensity occurred with the progression of dysplasia and with increasing excitation wavelength except at 780nm, as shown in Fig. 5(e) and Fig. 5(f).

#162351 - $15.00 USD Received 31 Jan 2012; revised 15 May 2012; accepted 15 May 2012; published 12 Jun 2012

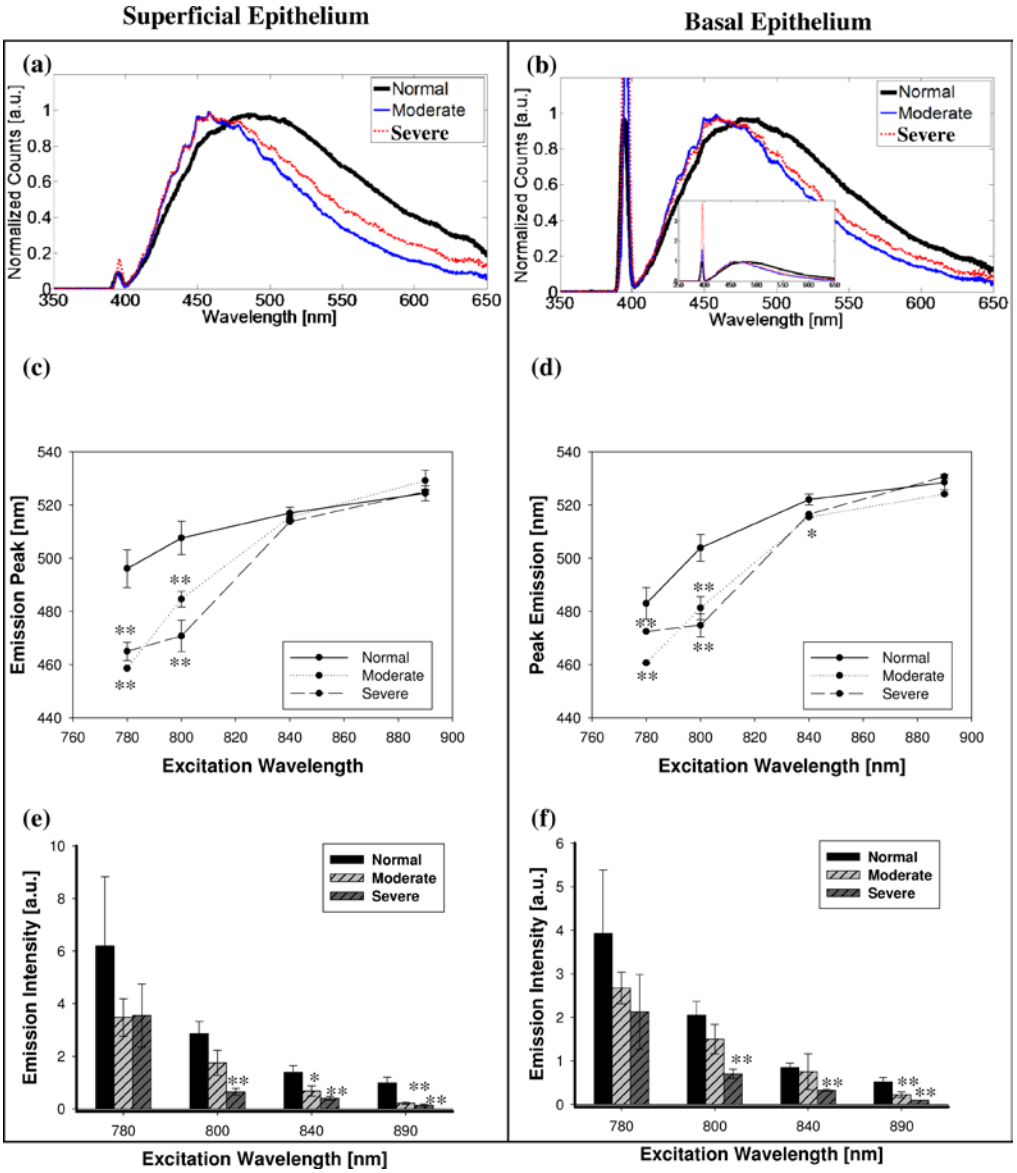


Fig. 5. Representative emission spectra plots for normal, moderate and severe oral mucosal tissue are shown in (a) and (b), at 780 nm excitation for the superficial and basal epithelium respectively. Plots (c) and (d) represent the emission peak position as a function of excitation wavelength for the different classifications. The total emission intensity of the three tissue grades are show for the superficial epithelium (e) and basal epithelium (f), at four excitation wavelengths. Level of significance is shown for moderate or severe relative to normal *($p < 0.05$), ** ($p < 0.001$).

### *3.4. Metabolic Activity*

The dominant fluorophores in the epithelium for 1P excitation ranging from 350 nm to 450 nm are the metabolic co-enzymes NAD(P)H and FAD [27,34]. Two-photon excitation at 780 nm is expected to elicit fluorescence from both NAD(P)H and FAD whereas excitation at 890 nm will elicit a signal primarily from FAD [34]. NAD(P)H emits in the 400 to 500 nm range with a peak near 450 nm at 780 nm excitation, while FAD emits in the 450 to 650 nm range with a peak at approximately 530 nm, for 890 nm excitation [34]. The redox ratio is a measure

#162351 - $15.00 USD Received 31 Jan 2012; revised 15 May 2012; accepted 15 May 2012; published 12 Jun 2012

cellular metabolic activity and can be determined from the ratio of the concentration of NAD(P)H relative to FAD [35]. An optically derived redox ratio was determined for 2P excitation of cellular regions within the epithelial layer of the oral mucosa at 780 nm and 890 nm excitation wavelengths. The spectra at these two wavelengths are represented by the red and blue spectral plots respectively in Fig. 6(a). Decoupling of the FAD contribution at 780 nm excitation was achieved by first equalizing the 780 nm and 890 emission spectra for $\lambda >$ 530 nm as shown in 6(a). This region of both spectra is attributable primarily to FAD fluorescence since the NAD(P)H contribution beyond this wavelength is extremely small [34]. Subtraction of the 890 nm plot from that of 780 nm results in the difference plot (green) of 6(a) which is due primarily to NAD(P)H. This is evidenced by the emission peak at approximately 450 nm and the spectral distribution from 400 nm to approximately 550 nm.

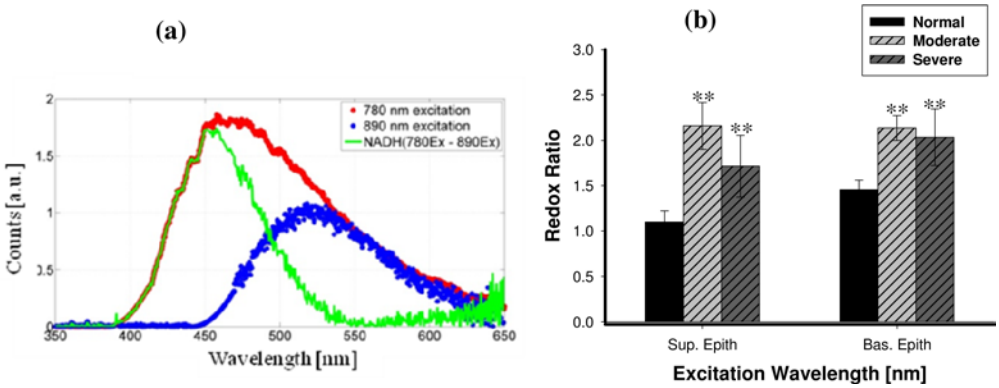


Fig. 6. (a) Spectral plots for 780 nm and 890 nm excitation of the epithelia layer of normal oral mucosa (red and blue plots respectively) are displayed. The green plot represents the difference between the two plots after normalization at longer wavelengths and represents the contribution due to NAD(P)H) only. The bar graph shown in (b) represents the redox ratio for the superficial and basal epithelium of normal, moderate and severe dysplasia of the oral mucosa, **($p<0.001$).

The optical redox ratio is defined here as intensity ratio of NAD(P)H/FAD and is represented in Fig. 6(b) for the different classification of oral mucosa. As defined, a higher ratio corresponds to higher cellular metabolic activity. Thus the results indicate greater metabolic activity for dysplasia relative to normal in both investigated layers.

### *3.5. Stromal layer*

Multiphoton micrographs of the upper stroma in normal, moderate, and severe dysplasia are shown in Figs. 7(a)–7(c). The well-defined fibrillar features of normal stroma are less well defined with the progression of dysplasia.

A strong SHG peak dominates the emission as seen in Fig. 7(d) (inset) and this is consistent with the expected response from type I collagen [32] a major component of oral mucosa stroma. In Fig. 7(d), the normalized emission spectra for all three classifications of oral mucosa have similar spectral distribution for 780 nm excitation. Nevertheless, a blue shift is also observed for this layer although the magnitude of the shift is small compared to the stratum corneum and epithelial layer as shown in Fig. 7(e). The peak shift at 800 nm allowed for differentiation between normal and dysplasia, in addition to distinction between the two abnormal mucosa classifications. The difference between normal and moderate dysplasia was statistically significant at all wavelengths except 840 nm, whereas the difference between normal and severe was significant only at 800 nm. For normal tissue, the autofluorescence signal is approximately two orders of magnitude smaller compared to the other layers. A significant decrease in the autofluorescence intensity between normal and dysplastic mucosa was observed at all four excitation wavelengths investigated.

#162351 - $15.00 USD Received 31 Jan 2012; revised 15 May 2012; accepted 15 May 2012; published 12 Jun 2012

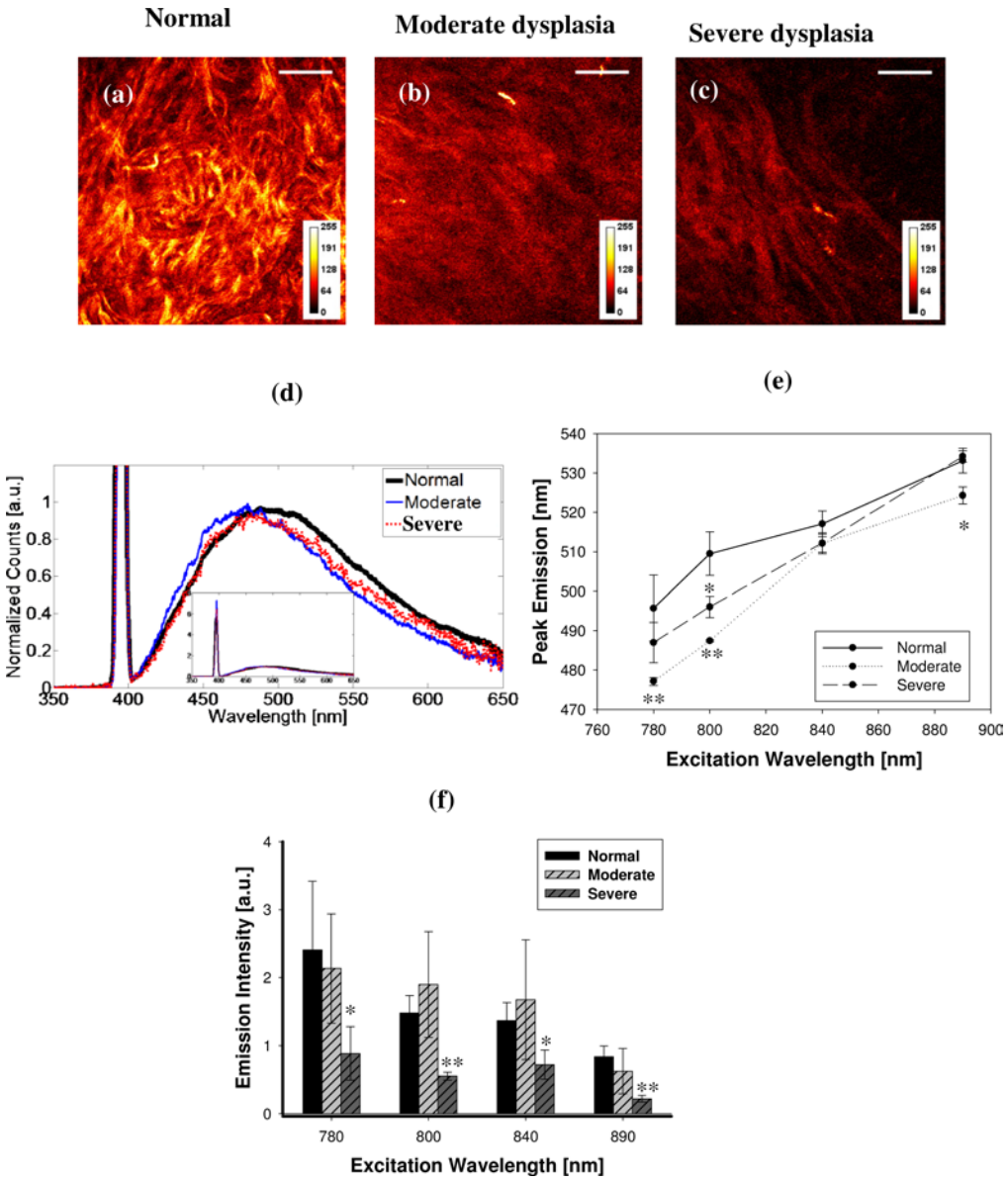


Fig. 7. Images (a) to (c) are 2P images of the stroma for normal, moderate and severe oral mucosa tissue. The normalized spectroscopy results for 780 nm excitation are represented in (d). Plot (e) represents the emission peak position as a function of excitation wavelength. Bar plot (f) depicts the emission intensity results. Scale bar in a-c is 50 µm. Level of significance is shown for moderate or severe relative to normal *($p < 0.05$), ** ($p < 0.001$).

A secondary peak was detected in the stroma near the SHG signal as shown in Fig. 8 for 890 nm excitation. A similar phenomenon has been previously reported in normal mouse skin tissue [33,36] and was attributable to a Raman shift. Our calculations for the relative wavenumber shifts are in close agreement to published results for a similar experiment [36]. It was observed that this peak is on average 3 times greater amplitude in both moderate and severe dysplasia compared to normal oral mucosa (n = 18). This result is interesting and should be further investigated to establish the potential of this signal as an indicator of the presence of dysplastic changes in oral mucosa and other epithelial tissue.

#162351 - $15.00 USD Received 31 Jan 2012; revised 15 May 2012; accepted 15 May 2012; published 12 Jun 2012

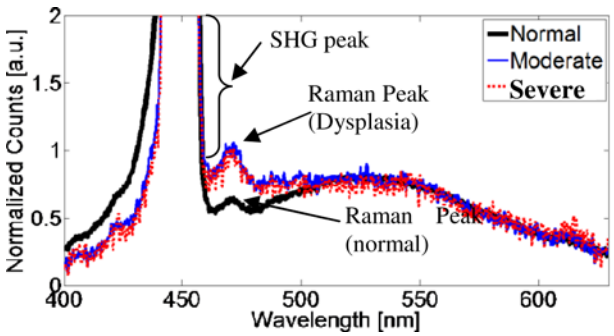


Fig. 8. Emission spectra for the stroma for normal, moderate and severe dysplasia oral mucosa at 890 nm excitation. A very strong SHG peak was observed in addition to a very weak Raman peak. A similar result was observed for 840 nm excitation of this layer.

## 4. Discussion

In this approach, two-photon spectroscopy was utilized for the layer-resolved in-vivo characterization of normal and precancerous oral mucosa. These preliminary results indicate specific differentiation in spectroscopic signals between normal tissue and dysplasia, both in intensity and in emission spectral peak characteristics. It is anticipated that this work will assist in defining future noninvasive assessment of neoplastic oral mucosa via nonlinear optical spectroscopy/microscopy. Additionally, results could be relevant to single photon spectroscopic assessment of oral mucosa. For example, while it has been reported in single photon spectroscopic studies that the emission intensity of the bulk mucosa is significantly reduced for dysplasia compared to normal [24], evidence presented using depth-resolved nonlinear spectroscopy reveals that this is also true for each individual layer investigated. Highly statistically significant changes were observed for specific wavelengths in each layer, reinforcing the notion of judicious wavelength selection for optimum detection and diagnosis of neoplastic change.

In the stratum corneum for example, a statistically significant decrease in emission intensity between normal and dysplasia (moderate and severe inclusive) was observed for all excitation wavelengths except at 780 nm (Fig. 3(f)). A similar trend was reported in one image-based study [10]. In the current study, it was possible to distinguish between normal and severe dysplasia at 800 and 840 nm, but not between normal and moderate dysplasia at these two wavelengths. However, all three classes were distinguishable at 890 nm based on intensity differences (Fig. 3(f)). This result suggests that 2P excitation wavelengths in the 800-890 nm range may be well suited for detecting precancerous changes of the outer layer of the oral mucosa, in agreement with previously published reports for 1P (i.e. 400-450 nm) confocal spectroscopy of oral cancer [23,37]. Differences in spectral peak characteristics were also noted in the stratum corneum. For example, the peak position of the normal mucosa emission was nearly constant at approximately 510 nm (Fig. 3(e)) with increasing excitation wavelength. This is in contrast with dysplasia where the emission peak position increased from approximately 480 nm at 780 nm excitation to 520 nm at 890 nm excitation (Fig. 3(e)). Thus although the dysplastic tissue is blue shifted relative to the normal mucosa at 780 nm, this shift decreased to zero at approximately 870 nm and is red shifted at 890nm. This observation can be explained on the basis of a significant increase in the keratin content. The emission spectra for the stratum corneum includes contributions from lipids such as phospholipids and lipofuscin which emit in the 540 nm range [38]. Given that pure keratin emits maximally at approximately 450 nm for 764 nm 2P excitation [30], the blue shift observed at 780 nm excitation (Figs. 3(d) and 3(e)) implies that the proportion of keratin increases with dysplasia. This is consistent with the onset of hyperkeratosis. The decrease in the shift with excitation wavelength is probably the combined effect of non-optimal excitation

#162351 - $15.00 USD Received 31 Jan 2012; revised 15 May 2012; accepted 15 May 2012; published 12 Jun 2012

of keratin and a slight increase in the contribution from other native fluorophores. Differentiation between normal and dysplasia was possible for the investigated wavelengths except at 840 nm based on the peak shift; but not between moderate and severe dysplasia at any investigated wavelength. Thus our results suggest that excitation of the stratum corneum at longer wavelengths ($\lambda > 800$) may allow for effective premalignant discrimination albeit at the expense of spectral separation of the emission signals.

The results for the epithelium can be understood in terms of the dominant fluorophores which are NAD(P)H and FAD. For example, at 780 nm up to approximately 820 nm (Figs. 5(a)-(b)), a significant blue shift of the emission spectra for the dysplastic mucosa relative to normal is observed. Given that both NAD(P)H and FAD are simultaneously excited at wavelengths near 780 nm and the emissions peaks are at 450 and 550 nm respectively, this shift is indicative of an increase in the proportion of NAD(P)H relative to FAD. This in turn implies a higher redox ratio and higher metabolic activity with dysplasia in agreement with expectation. Decoupling of the NAD(P)H signal at 780 nm revealed that the emission intensity of this metabolic co-enzyme is lower for dysplastic oral mucosa relative to normal tissue in both the superficial and basal epithelium (data not shown). However, this decrease was found to be statistically significant only between normal and severe epithelial dysplasia. A similar decrease in NAD(P)H intensity has been reported for human oral carcinoma studies [39]. At longer excitation wavelengths approaching 890 nm, primarily FAD is excited. Thus the emission peak separation is negligibly small at these wavelengths. This accounts for the trend in Figs. 5(c) and 5(d). Statistically significant spectral shifts between normal mucosa and dysplasia ($p < 0.001$) are readily apparent for the shorter wavelengths, however statistically significant differences in the emission intensity are observed for longer excitation wavelengths as seen in Figs. 5(e) and 5(f). Quite interesting, it was possible to distinguish between the two classes of dysplasia ($p < 0.05$) at 780 nm and 800 nm in the epithelium. Therefore, the optimum excitation wavelength for discrimination between normal and dysplastic mucosa in this layer appears to be 800 nm, since it simultaneously allows for good spectral separation and intensity based differentiation. We intend to confirm this in an expanded study in the near future.

Reports on the utilization of 2P imaging and FLIM measurements for redox ratio estimation have been published [27,34,35]. In the current work, we utilized point measurements to determine this value with strong agreement with previously published results for dysplasia of the oral mucosa [27]. A statistically significant increase in the redox ratio was observed for both moderate and severe dysplasia when compared to normal (Fig. 6(b)). However, it was not possible to differentiate between the two classes of dysplasia using this parameter. It is interesting to note that a statistically significant difference in the redox ratio between the superficial and basal epithelium was detected for normal but not for dysplasia. This is consistent with the idea of a more homogenous distribution of cells with increased metabolic activity within this layer, with the progression of dysplasia. Overall, it appears that single wavelength excitation at 890 nm for class discrimination (Figs. 5(e)–5(f)) may be as efficacious as dual (780nm and 890 mm) excitation of the oral mucosa which is required for redox ratio determination.

The autofluorescence signal from the stroma is very weak compared to that of the overlying keratinizing and epithelial layers. However, similar trends for the emission peak position (Fig. 7(d)) and intensity distribution (Fig. 7(e)) are observed. Although smaller, a blue shift was also detected for this layer as reported for the stratum corneum and epithelial layer, but the origin is not as clear. A statistically significant intensity difference between normal and severe dysplasia was observed for each excitation wavelength but not for normal and moderate. It is possible that these results may be influenced by scattering and absorption at this depth [40] and further research is required to ascertain the origin of the observed spectral differences. A very strong SHG signal was detected in the stroma but the amplitude was not correlated with the progression from normal to dysplasia, nor was the ratio of

#162351 - $15.00 USD Received 31 Jan 2012; revised 15 May 2012; accepted 15 May 2012; published 12 Jun 2012

SHG/AF (autofluorescence), as recently reported [41]. A weak SHG signal was detected in the epithelium (Fig. 5(a)) and attributed to epithelial DNA [28,42]. Other reports have confirmed the presence of a SHG signal in the epithelium [43]. The detected SHG signal in the basal epithelium (Fig. 5(b)) likely originates from the underlying stromal collagen given that this layer is very thin. Since this signal is not present in the stratum corneum, the amplitude of this peak may be used for single acquisition point layer discrimination in the absence of imaging. We found that the ratio of the SHG to autofluorescence amplitude was excellent for determining the layer of signal acquisition, and that this metric was sensitive enough to differentiate between the superficial and basal epithelium (data not shown).

An extraneous small peak was observed near the SHG peak as shown in Fig. 8 for 890 nm excitation of the stroma (also at 840 nm not shown) and is possibly a Raman peak. Such a phenomenon has been reported for *in vivo* 2P spectroscopic characterization of mouse skin [36]. We observed a shift of the emission peak with excitation wavelength, and the presence of Stoke and anti-Stoke shifted peaks centered at the SHG peak. When converted to wavenumbers, a constant difference between the emission peak and SHG maxima was observed. The wavelength shifts were determined to be $1751 \pm 117$ $cm^{-1}$ for the Stoke shifted peaks and $987 \pm 77$ $cm^{-1}$ for the anti-Stoke peaks for the normal mucosa, in agreement with published findings in mouse skin [36]. The amplitude of this new peak was about three times greater with dysplasia than in normal mucosal tissue and further studies are planned to confirm this relationship.

In summary, the results of this preliminary study indicate that non-linear optical spectroscopy based on intrinsic signals may facilitate discrimination of different grades of dysplasia. While previous studies have examined individual spectral windows using multiphoton microscopy, the spectroscopic assessment conducted in the current study is helpful in defining the specific layer-resolved spectral and intensity changes that occur with dysplasia over multiple excitation wavelengths. Such knowledge could be highly useful toward the development of diagnostic approaches for oral precancers and cancer. From a basic perspective, it could be of interest to assess the earliest changes in a depth/layer-resolved manner in order to gain a better understanding of alterations at multiple layers of interest which may take place in neoplastic transformation. From a clinical perspective it may be of interest to specifically detect high-risk lesions which could be surgically removed, which generally include those with severe dysplasia. This study demonstrates a number of spectral possibilities that could be used to identify intensity or peak shift changes, the choice of which will be highly dependent upon the goal of detection and modality available. It will be of interest to investigate the changes beyond dysplasia to include oral squamous cell carcinoma and to exploit multivariate layer-resolved analysis for sensitivity and specificity evaluation of non-linear spectroscopy. This is important because notwithstanding the significant advancements in the application of linear spectroscopy techniques for the assessment of precancerous and cancerous alterations of the oral mucosa, full clinical translation is yet to be realized. It has been speculated that increased absorption and scattering due to increased micro-vascularization, changes in refractive index and thickening of the keratinizing layer (hyperkeratosis) may account for some of these limitations [24,44]. Although 2P spectra will also be strongly influenced by these factors, the effect is likely to be less compared to 1P. A significant aspect of this study is that differentiation between normal and dysplasia, and even between different classifications of dysplasia was possible via examination of micro-regions. It is interesting to note that very little variation was observed between the three spectra acquired per investigated site when multiple measurements of the individual sites were analyzed for differences by ANOVA. These results are potentially important because of the implication that differentiation may be possible by sampling a few points instead of the full-field/large region of interest approach. Nonetheless it may be of interest to examine full field of view variations via pixel-by-pixel spectroscopic analysis of the sampled field.

#162351 - $15.00 USD Received 31 Jan 2012; revised 15 May 2012; accepted 15 May 2012; published 12 Jun 2012

## 5. Conclusion

Oral dysplasia was investigated for the first time via two photon AF and SHG spectroscopy at multiple excitation wavelengths. Statistically significant changes were observed for all four investigated layers. In general, the spectra of the dysplastic mucosa are blue-shifted relative to normal, with the magnitude of this shift decreasing with increasing wavelength and depth. Analysis of the epithelial layer indicated a statistically higher redox ratio in the dysplastic mucosa for both the superficial and basal epithelium compared to normal. A statistical difference in the redox ratio between the superficial and basal epithelium was detected for normal but not for the moderate and severe dysplasia, consistent with the expectation of decreased metabolic differentiation in depth during pre-neoplastic transformation. In the case of the stroma, it was possible to differentiate between normal and dysplastic tissue based on autofluorescence changes but not via analysis of SHG signals. These preliminary results will serve to guide future 2P spectroscopy studies by helping to establish sensing parameters for precancerous changes in epithelial tissue, and may also provide some insight into the signal origin in 1P spectroscopy as well as the development of diagnostic tools in precancer/cancer imaging.

## Acknowledgments

Contributions from Tuya Shilagard (T. S) and Jinping Yang (J. Y) are acknowledged for development and maintenance of the animal model (T. S., J. Y.), and assistance in intravital imaging (T. S., J. Y.) during spectroscopy. We are thankful for their assistance. The authors would like to acknowledge funding for this research from the National Institutes of Health (NIH) through the award of the grant no. NCI R01CA127429.

#162351 - $15.00 USD Received 31 Jan 2012; revised 15 May 2012; accepted 15 May 2012; published 12 Jun 2012